Bachelor Thesis

Temporal evolution of the surface temperature distributions on isolated strongly magnetized neutron stars

written by

Sabrina Gronow

University of Bremen

Department of Physics and Electrical Engineering

Matriculation nr. 2693611

sgronow@uni-bremen.de

September 3, 2014

in Cooperation with the German Aerospace Center (DLR e.V.)
Institute of Space Systems
Department for System Conditioning

Evaluators:
Prof. Dr. U. R. M. E. Geppert (DLR)
Priv.-Doz. Dr. A. Ladstätter-Weißenmayer (University of Bremen)

Contents

List of Figures

Acknowledgement

I am particularly grateful to Prof. Dr. Geppert who made it possible for me to write my Bachelor thesis at the German Aerospace Center. His willingness to give his time so generously has been very much appreciated. The talks and hints helped a lot in the finishing of this work. I further want to thank Priv.-Doz. Dr. Ladstätter-Weißenmayer for her very helpful advice and assistance.

I would like to express my thanks to Farid Gamgami and Marco Scharringhausen who made the contact to the German Aerospace Center. Thereby I thank the German Aerospace Center for the permission of my work.

Finally I want to thank everyone who advised me of something or gave me moral support.

Sabrina Gronow, September 3, 2014

Abstract

About 10^8 neutron stars exist in our milky way. Isolated neutron stars build a subgroup of this stellar group and they are thermally cooling neutron stars. As they describe the only possible structure – apart from black holes and white dwarfs – that can develop after a stellar collapse, researchers focus on the determination of their characteristics.
In this work the influence of the magnetic field configuration onto the surface temperature distribution is analysed in consideration of two different magnetic field models. In one case it is core threaded and in the other crust confined. The evolution of these fields is calculated over approximately $1 \cdot 10^7$ years. Short films that demonstrate the effect of two different evolving magnetic field configurations onto the surface temperature distributions are main results of the thesis presented here.
The analysis reveals that a toroidal and meridional magnetic field structure prevents an outward heat flux, whereas a radial magnetic field component encourages the heat transfer. The temporal stability as well as the individual surface temperature distribution are discussed. In future work the magnetic field of existing neutron stars can be determined via the influence the surface temperature distribution has on the pulse profile which can be detected through X-ray observations.

Kurzbeschreibung

Etwa 10^8 Neutronensterne existieren in unserer Milchstraße. Isolierte Neutronensterne bilden eine Untergruppe dieser Sternklasse. Sie sind thermisch abkühlende Neutronensterne. Da sie neben Schwarzen Löchern und Weißen Zwergen die einzige Struktur beschreiben, die nach einem stellaren Kollaps entstehen kann, widmen sich Forscher der Bestimmung ihrer Eigenschaften.
In dieser Arbeit wird der Einfluss des Magnetfeldes auf die Oberflächentemperaturverteilung bei zwei verschiedenen Magnetfeldmodellen untersucht. In einem Fall durchdringt das Feld den gesamten Stern und im anderen Fall nur die Kruste. Die Entwicklung dieser Felder wird für etwa $1 \cdot 10^7$ Jahre berechnet. Kurzfilme, welchen den Effekt zweier verschiedener Magnetfeldentwicklungen auf die Oberflächentemperaturverteilungen zeigen, sind die Hauptergebnisse in der hier dargelegten Arbeit.
In der Analyse ergibt sich, dass die toroidalen und meridionalen Magnetfeldstrukturen den nach außen gerichteten Wärmefluss behindern, während der Wärmetransport durch eine radiale Magnetfeldkomponente unterstützt wird. Die zeitliche Stabilität sowie die individuellen Oberflächentemperaturverteilungen werden diskutiert.
In künftigen Arbeiten kann das Magnetfeld existierender Neutronensterne über den Einfluss der Oberflächentemperaturverteilung auf das Pulsprofil rotierender Neutronensterne, welches aus Beobachtungen der Röntgenstrahlung ermittelt werden kann, bestimmt werden.

1 Introduction

There are three possibilities for stars to end after their collapse. They either become white dwarfs, neutron stars or black holes. All three of these are compact objects. The process depends on the individual stellar mass before the collapse. If the mass is in the range of about 1.4 to 8 solar masses the star turns into a neutron star. A lower mass results in a white dwarf, whereas a higher mass leads to a black hole. However the limits haven't been determined for certain yet. Other factors such as an existing magnetic field or a rotation can also have an influence. Thus a further analysis of the parameters involved in the development is necessary. The formation of a new star can take up to 10^7 years depending on the mass of the initial star [1].
This thesis is going to focus on neutron stars in particular which have a mass of approximately $1.4\,M_{\odot}$ after the collapse. In the progress of the formation of the neutron star some of the original stellar matter remains as interstellar gas. Therefore neutron stars only have a fraction of the mass of the original star [1]. Isolated neutron stars form a sub-group in this category of stars. They are thermally cooling neutron stars, not necessarily spatial isolated as the name might suggest [2].

A collapse occurs when a star is dying, for example when the nuclear fuel is depleted. In this case the stellar matter heats up and a high amount of γ-radiation is discharged. Due to this γ-radiation photodesintegration takes place which can lead to the disposal of α-particles or neutrons. These α- and γ-particles form protons p and neutrons n in a reaction based on $\alpha + \gamma \rightarrow 2p + 2n$ [3]. The radiation pressure working against the gravitational pressure vanishes and thereby leads to the intense compression of the core [1]. In case of a forming neutron star the existing electrons and protons fuse together. The so-called electron capture happens at high densities according to the inverse β-decay reaction (see equation 1), with electron e^-, proton p, neutrino ν_e and neutron n.

$$e^- + p \rightarrow \nu_e + n \tag{1}$$

The degeneracy pressure of the neutrons stops the collapse [1]. But during this process in-falling material is reflected by the core and collides with other stellar matter from further outside. That way the outer layer of the former star is pushed off. This leads to the supernova explosion one can observe from the earth [1].

According to the proposition of Baade and Zwicky in 1934 about the idea of neutron stars, the first neutron star was discovered in 1967 as pulsar or rotating neutron star [4]. Up to now about 2000 pulsars are known, although as many as 10^8 are assumed; one example is the famous Crab pulsar [5].
Neutron stars have a radius of about 10 km. As a consequence of it and their high mass the compact objects have densities of $(10^8 - 10^{15})\frac{\mathrm{g}}{\mathrm{cm}^3}$. Furthermore neutron stars can have magnetic fields of the order of 10^{12} G to 10^{15} G [6]. The strong magnetic field originates from the contraction of the plasma. During the contraction the initial weak magnetic field of charged particles becomes compressed [1]. It is assumed that there is a connection between this strong magnetic field and the surface temperature distribution of the neutron star. But because up to now only very little is known about the interior magnetic field configuration, new achievements can only be made by considering the effect of the magnetic field on the heat flux or the density profile. These results can be compared to observations or different model calculations.
In this work two different structures of the magnetic field are considered; a crust confined and a core threaded magnetic field. Each of these models consists of a dipolar poloidal and a dipolar toroidal component. The influence of these magnetic fields onto the heat flux is studied in order to examine the dependence more closely.
In the following sections fundamental assumptions about the neutron star structure (section 2.1) as well as the theoretical basics for the considered models are listed (section 2.2). Furthermore theoretical, mathematical main features are given in two sections about the magnetic field effects (section 3) and the magneto-thermal evolution (section 4). Subsequent to this the temporal evolution of the surface temperature distributions of the two considered models is illustrated, explained (section 5) and discussed (section 6).
See *Black Holes, White Dwarfs and Neutron Stars: The physics of compact objects* by S. L. Shapiro, S. A. Teukolsky (2004) for more detailed information on compact objects [7].

2 Fundamental assumptions

Neutron stars are so far the densest known stars in the universe [8]. They have a typical radius R_{NS} of about 10 km. In the following subsections the inner structure of the neutron star considered in the model calculations and the fundamentals of the analysis in this work are specified.

2.1 Structure of a neutron star

In figure 1 the inner structure of a neutron star with a radius of 10.6 km is shown. It is assumed that the star can be divided into four different main parts, the outer crust, inner crust, outer core and inner core.

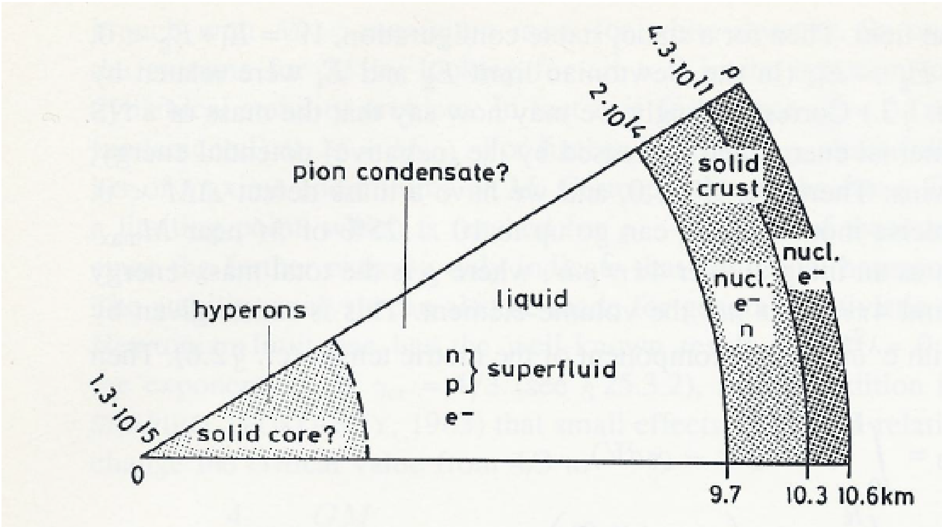

Figure 1: The inner structure of a neutron star [9].

If not mentioned explicitly the theory of the inner structure is taken from Kippenhahn et al. (2012) [9].
The outer crust has a depth of only a few hundred meters and consists mainly of nuclei and electrons. The density is at about $4 \cdot 10^{11} \frac{\text{g}}{\text{cm}^3}$. Below this layer the neutron fraction increases to the center [1]. In the inner crust the density increases up to a value of $2 \cdot 10^{14} \frac{\text{g}}{\text{cm}^3}$. A liquid of neutrons, nuclei and electrons exists. At the boundary to the outer core all nuclei are dissolved. The inner and the outer crust are displayed as medium and fat shaded areas in figure 1 respectively. Above the outer crust a thin envelop exists which has an even smaller density than the outer crust.
The outer core (not shaded in figure 1) begins at a radius of about 9.7 km and has a density higher than $2 \cdot 10^{14} \frac{\text{g}}{\text{cm}^3}$. It is comprised of free neutrons, electrons, and superconductive protons. At temperatures T below 10^{11} K the neutrons become superfluid [1].
The structure of the inner core is unknown yet. It is illustrated as lightly shaded in figure 1. The density of $1.3 \cdot 10^{15} \frac{\text{g}}{\text{cm}^3}$ is higher than the density of a free nucleon which is just $2 \cdot 10^{14} \frac{\text{g}}{\text{cm}^3}$. It is assumed that a quark-gluon plasma is in the center of the star [1]. Even though, a solid core is possible as well.

2.2 Fundamentals and graphical illustration

In order to confirm the assumption of a magnetic field dependent surface temperature distribution already mentioned in section 1 a neutron star with a radius of $R_{NS} = 11.45\,\mathrm{km}$ is considered. The core-crust boundary (at radius R_B) is defined as the radius at which the density of a neutron ($\rho_n \approx 2 \cdot 10^{14} \frac{\mathrm{g}}{\mathrm{cm}^3}$) is present in the star. The initial temperature is uniformly given by $T(t=0) = 10^{10}\,\mathrm{K}$ in the core and crust.

The models considered here postulate a vacuum outside of the star. In order to create a purely crustal field, the protons in the core have to be in a superconducting state. In that case the Meissner-Ochsenfeld effect prevents the magnetic field to penetrate the core. In case the magnetic field permeates the whole star the electric conductivity in the core is assumed to be many orders higher than in the crust. This leads to a higher decay time for the currents in the core than for those in the crust.

The external magnetic field is dominated by the dipolar poloidal component in both cases. This external poloidal field is determined by the strength of the magnetic field at the poles. This assumption is made corresponding to Geppert et al. (2006) [10].

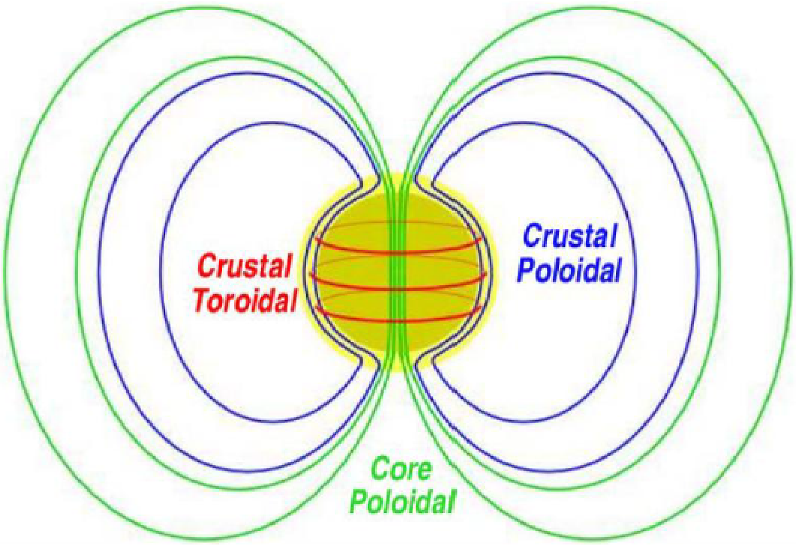

Figure 2: Graphical visualization of the different magnetic field components [11].

The graphical visualization of these structures is shown in figure 2. Assuming values of about $B_{pol}(r = R_{ns}, \theta = 90°, t = 0) = 10^{13}\,\mathrm{G}$ and $B_{tor,max,core}(t = 0\ ) = 2 \cdot 10^{16}\,\mathrm{G}$ and $B_{tor,max,crust}(t = 0) = 1.5 \cdot 10^{15}\,\mathrm{G}$ for the poloidal and toroidal components of the core and crustal magnetic field respectively. The neutron star has to be considered as strongly magnetized.

The surface temperature distributions and magnetic field structures over a timespan of 10 million years are calculated and provided by Prof. U. R. M. E. Geppert using an explicit code by the Alicante group [12]. It is based on the finite difference method and gives solutions for a system of coupled second order partial differential equations. This code can solve the field evolution considering a very low magnetic diffusivity and the formation of sharp current sheets [13].
The movement of the magnetic field and the formation of magnetic spots is caused by the Hall drift. But the direction of that shift is determined by the geometry of the toroidal field component at the beginning of the calculations (t=0). In the considered dipolar toroidal structure in the core model, the poloidal field is moved toward the North pole and the initial equatorial symmetry is broken.
The resulting values of the surface temperature T_s in dependence of the angle θ between the North and the South Pole were extrapolated onto the whole stellar surface due to the axial symmetry. The values were calculated for 49 different angles between $-88.6994°$ and $88.7055°$. At the poles ($-90°$ and $90°$ for the North and the South Pole respectively) the values of the neighbouring calculated angles are assumed. The equator is described with $\theta = 0°$ and $\phi = [-180°, 180°]$. See figure 3 for a display of the different angles.

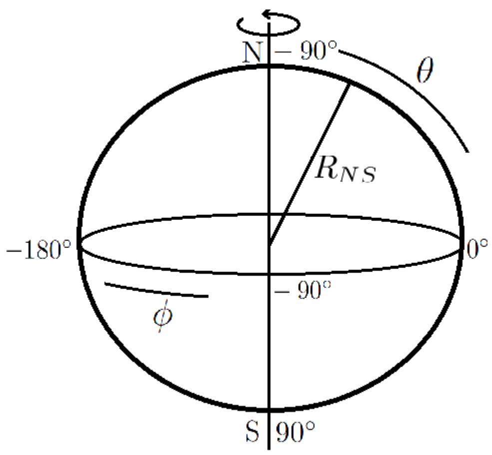

Figure 3: Display of the angle relations.

The graphical illustration of the surface temperature distribution is operated with the MatLab Program. The Code is given in the appendix (see page 26 and following). The two dimensional representation of the three dimensional neutron star is carried out in a sinusoidal projection. The North Pole is located in the middle of the left half, whereas the South Pole is on the right side. Both are marked by the letters N and S, respectively.

The initial small number of data points leads to a blur in the visualisation. A linear interpolation between each point results in a better representation.
A short film is generated for each model with the surface temperature distribution and the corresponding magnetic field structure next to each other in order to alleviate the analysis of the causality. In the illustration of the magnetic field the crust is enhanced compared to the rest of the star. This further illustrates the changes in these areas.
The compiled images are joined together in a video for each model. These videos can be found on the DVD in the appendix.
After the calculated 10 million years a stationary state is reached.

3 Magnetic field effects on heat flux and tensor of heat conductivity

The temperature distribution of the neutron star is affected by the magnetic field. Either the magnetic field has an influence as a Joule heat source or the magnetic field lines change the direction of the heat flux [13]. The following section is going to focus on the effect of the magnetic field lines on the heat flux.
In 2004 and 2006 Geppert et al. discussed several possible magnetic field configurations ([6], [10]), just as Yasutake et al. did in 2014 [14]. Considerations were made regarding a simple poloidal core and crustal field as well as a superposition of these components with a toroidal field.
The magnetic fields analysed in this thesis consist of a dipolar poloidal and a dipolar toroidal component. Once permeating the whole star, once not. The mathematical equations which give the different field components in spherical coordinates and considering axial symmetry are taken from Geppert (2013) [11]:

$$\vec{B}_{pol}(r,\theta,t) = B_r(r,\theta,t)\vec{e}_r + B_\theta(r,\theta,t)\vec{e}_\theta$$
$$\vec{B}_{tor}(r,\theta,t) = B_\phi(r,\theta,t)\vec{e}_\phi$$

The magnetic field has a huge impact on the temporal thermal evolution of the star. Without a magnetic field the temporal evolution of the temperature T proceeds according to the energy balance equation (equation 2) and the heat transport equation (equation 3) [6]:

$$C\frac{\partial T}{\partial t} = -\nabla \cdot \vec{F} \tag{2}$$
$$\vec{F} = -\kappa \cdot \nabla T \tag{3}$$

with C as specific heat per unit volume, the heat flux density $\vec{F}$ and $\kappa = \kappa_0$ the scalar heat conductivity if there is no or only a very weak magnetic field. In the energy balance equation it is assumed that the neutron star does not contain any heat sources or sinks itself. In this case there would be an isotropic heat flux $\vec{F} = F(r)\vec{e}_r$.

When a magnetic field exists the scalar heat conductivity becomes a 3×3 tensor and the heat flux is dependent on θ as well considering axial symmetry (equation 4).

$$\vec{F} = F(r,\theta)\vec{e}_r + F(r,\theta)\vec{e}_\theta \tag{4}$$

In this case κ is given by equation 5 with the components in equations $6a - c$. The heat conductivity becomes dependent on the magnetic field.

$$\kappa = \hat{\kappa}(r,\theta,t,B) = \begin{pmatrix} \kappa_\perp & \kappa_\wedge & 0 \\ -\kappa_\wedge & \kappa_\perp & 0 \\ 0 & 0 & \kappa_\parallel \end{pmatrix} \tag{5}$$

The vector and tensor components are described as relative to the magnetic field vector $\vec{B}$.
The parallel, perpendicular and Hall component of the conductivity tensor are given by the equations $6a - c$:

$$\kappa_\parallel = \kappa_0, \qquad \kappa_\perp = \frac{\kappa_0}{1 + (\omega_B \tau)^2}, \qquad \kappa_\wedge = \omega_B \tau \kappa_\perp \tag{6a - c}$$

with $\kappa_0 = \frac{\pi^2 k_B^2 T n_e \tau}{3 m_e^*}$ as scalar heat conductivity. A similar structure for the electric conductivity σ arises, too. The parameter m_e^* describes the effective electron mass and $n_e = \frac{\rho Z}{A m_u}$ the number density with the atomic mass unit m_u [15].

$$\omega_B = \frac{eB(r,\theta,t)}{m_e^*(r)c} \tag{7}$$

The components of the heat conductivity depend on the magnetization parameter $\omega_B \tau$, with ω_B given by equation 7 and relaxation time τ between two particle collisions, which can vary over several orders of magnitude in the crust. Furthermore the magnetization parameter plays an important role in the temporal evolution of the magnetic field. A more detailed discussion can be found in section 4.2 in context with the Hall induction equation. A dependence on characteristics such as temperature, thermodynamic phase and chemical composition of the matter is nevertheless already obvious in this context due to the dependence on the parameters m_e^*, B and $\tau = \tau\left[\rho(r), T(r,\theta,t), Q(r), A(r), Z(r)\right]$, with density ρ, charge number Z, mass number A and impurity concentration Q [13].

In case of a negligible magnetic field the heat flows isotropically radial outwards. With $\kappa_{\|} = \kappa_0 \gg \kappa_{\perp}$ for $\omega_B \tau \gg 1$ in case of a strong magnetic field the heat flows parallel to the magnetic field lines. For this case Geppert et al. (2004) illustrated that a crustal field prevents the heat transport to the outside of the star, whereas a core field supports this transfer [6]. This is caused by the different structures of the models, the radial orientated field lines in a core field are a contrast to the meridional field lines in a crustal field.

When a crustal field is assumed, the pole is warmer than the equator due to the mentioned meridional structure. Most of the heat leaves the star at the poles. However according to considerations regarding the orientations of both the magnetic field and the temperature gradient the second thermodynamic law is not violated.

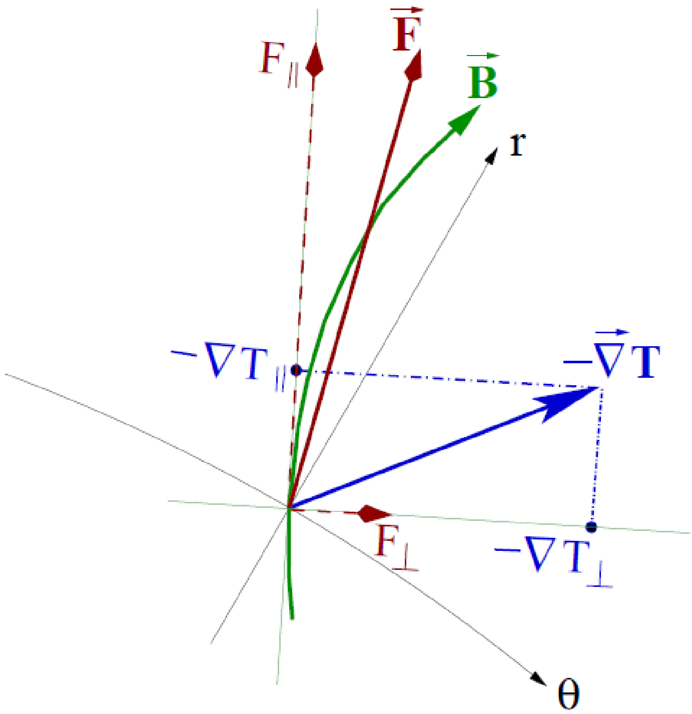

Figure 4: Vector relations of the magnetic field and heat flux [6].

Due to the fact that the heat conductivity tensor is positive definite it ensures that the product $\vec{F} \cdot \nabla T < 0$ at all times. For clarification: When $\vec{B}$ and the temperature gradient are perpendicular to each other in the northern hemisphere, the component $-\nabla T_\theta$ points toward the equator. As a result $-\nabla T_{\|} < -\nabla T_{\perp}$ and $\|F_{\|}\| > \|F_{\perp}\|$

with $F_\parallel = -\kappa_\parallel \nabla T_\parallel$, $F_\perp = -\kappa_\perp \nabla T_\perp$ and $\kappa_\parallel \gg \kappa_\perp$. Following from that the heat flux points towards the pole. See figure 4 for a graphical illustration.
The vector components are given relative to the magnetic field vector $\vec{B}$ corresponding to the components of the heat conductivity κ.
The theory used here is based on the thoughts and results of Geppert et al. (2004) [6] and Yakovlev and Kaminker (1994) [8].

4 Magneto-thermal evolution of isolated neutron stars

The magnetic field of a neutron star itself is maintained by currents which flow around the core and in the crust. Considering only the currents in the core, the Ohmic decay would not change the magnetic field much in time. In this case the decay time is given by $\tau_{Ohm} = \frac{4\pi\sigma L^2}{c^2}$, with electric conductivity σ and scale of the magnetic field L which is equivalent to about one half of the radius. According to Geppert (2013) the decay time of the core field is of the order of 10^8 years or even larger, whereas the crustal field characteristic decay time is 10^6 years [11]. Consequentially, it means that the crustal field evolves much faster than the core field. Thus the changes in the global neutron star magnetic field on typical radio pulsar lifetimes of $1 \cdot 10^7$ years are mainly a consequence of the change in the crustal field.
According to Geppert et al. (2013) the Hall drift effect is the only mechanism that can provide the strong and small scale magnetic fields assumed for neutron stars which appear as radio pulsars [13]. The Hall effect combines both poloidal and toroidal magnetic field component. The numerical calculations regarding the crustal and core magnetic field were made considering the Hall drift. This effect has a huge influence on the dynamics of the magnetic field and will be discussed in the following two subsections in detail.

4.1 Heat transfer equation

The heat flux is described by the heat transport equation (see equation 3). Corresponding to the thoughts of Geppert et al. (2004) the heat flux can be written in notation of the parallel, perpendicular and Hall components of the temperature gradient relative to the direction of $\vec{B}$ [6]. Considering the heat conductivity tensor (equations 5 and $6a-c$)

the resulting equation is

$$\vec{F} = -\hat{\kappa} \cdot \nabla T = -\frac{\kappa_0}{1 + (\omega_B \tau)^2} \times \left[\nabla T + (\omega_B \tau)^2 \cdot \vec{b} \cdot (\nabla T \cdot \vec{b}) + \omega_B \tau \cdot \vec{b} \times \nabla T\right] \quad (8)$$

with the normalized vector $\vec{b} = \frac{\vec{B}}{\|\vec{B}\|}$.

The Hall component of the temperature gradient is given by $(\nabla T)_\wedge = \vec{b} \times \nabla T$. By this the last term on the right hand side can be associated with the Hall component. This term is divergence free if the magnetic field and temperature gradient are axial symmetric. Furthermore it is proportional to the magnetization parameter $\omega_B \tau$. The component parallel to the magnetic field is given by $(\nabla T)_\| = \vec{b} \cdot (\nabla T \times \vec{b})$ and the perpendicular component by $(\nabla T)_\perp = \vec{b} \times (\nabla T \times \vec{b})$.

4.2 Hall induction equation

The temporal magnetic field evolution is based on one of Maxwell's equations, the induction equation. Considering the Hall effect the Hall induction equation is given by equation 9.

$$\frac{\partial \vec{B}}{\partial t} = -\frac{c^2}{4\pi} \nabla \times \left\{ \frac{1}{\sigma} \left[\nabla \times \vec{B} + \omega_B \tau ((\nabla \times \vec{B}) \times \vec{b})) \right] \right\} \quad (9)$$

It is a result of the tensorial character of the electric conductivity which is – in relaxation time approximation – exactly the same as for the heat conductivity. A more detailed specification would exceed this thesis.
The original induction equation is extended by an additional term which includes the Hall drift (last term on the r.h.s.). This non-linear effect is caused by the interactions of the magnetic field with the electric currents in the neutron star that maintain this magnetic field. Also, Pons and Geppert (2010) stated that an instability of the magnetic field caused by the Hall drift occurs if the magnetization parameter is high [16]. According to their assumption of a one-component plasma the conditions may be realized in the crust of a neutron star.
According to Rheinhardt and Geppert (2012) the effect of ambipolar diffusion can take place as well [17]. It does not occur in the solidified crust in this case because it is assumed that only electrons and one kind of immobile ion exist in the conducting matter; no neutral particles are present.
In the considered models two boundary conditions are given. A vacuum shall be present outside of the star. Hereby the magnetic field is free of any curls further outside the

crust. Besides that, the core is assumed to be a superfluid conductor in case of the crustal field. It shall be a perfect conductor. Due to the resulting Meissner-Ochsenfeld effect the magnetic field cannot penetrate into the core. Also crustal currents are constrained from permeating the core. It might however be possible that a core field exists in the form of flux tubes [7]. This field would evolve during a much longer time scale. The influence on the surface temperature would only be small in comparison and could be neglected.
In case of the core field it is assumed that the electric conductivity in the core is much higher than in the crust. In that case it evolves on time scales exceeding the typical radio pulsar lifetime of $1 \cdot 10^7$ years.

Taking a closer look at the Hall term in the Hall induction equation (equation 9) it is ascertainable that the intensity of the Hall drift is determined by the parameter $\omega_B\tau$. If $\omega_B\tau < 1$ the term is negligible small in comparison to the first term in the equation. Nevertheless if $\omega_B\tau \gg 1$ the Hall drift dominates the (normal) Ohmic dissipation which is represented by the left term on the r.h.s.. Pursuant Geppert et al. (2013) the magnetization parameter may locally and temporally exceed even values of 1000 [13]. In this case the perpendicular component of the electric conductivity is suppressed by a factor of at least 10^6. The Hall drift, which originates in the electron movement in the star, causes the temporal evolution of the magnetic field and as such describes the development of the magnetic field lines.
With the parameters $m = \frac{c^2}{4\pi}$ and $n = \frac{\omega_B\tau}{\sigma \cdot \|\vec{B}\|}$ the equation can be simplified to

$$\frac{\partial \vec{B}}{\partial t} = -m \cdot \nabla \times \left[n \cdot ((\nabla \times \vec{B}) \times \vec{B}) \right]$$

in case of a vanishing Ohmic resistivity which occurs in consideration of a perfect conductor in the crustal model.

5 Surface temperature distribution for different magnetic field configurations

As indicated in the previous sections the surface temperature distribution of a neutron star depends on the magnetic field structure. In order to validate this statement two different magnetic field structures are compared with the corresponding surface temperature distribution.

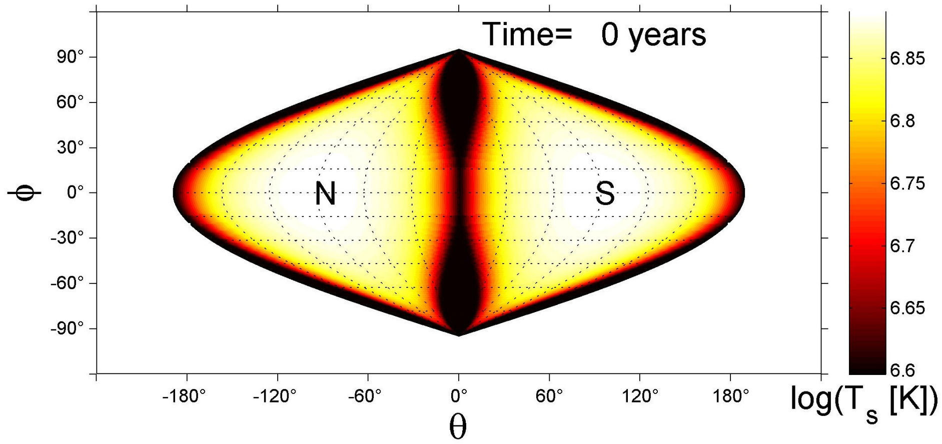

Figure 5: Initial surface temperature distribution of a neutron star of the core threaded and crust confined model.

In the following two subsections a magnetic field with a dipolar poloidal and a dipolar toroidal crustal field component will be considered. In one case the dipolar poloidal component penetrates the whole star, in the other it is confined to the crust of the neutron star. The first case is called a core field and the second a crustal field.

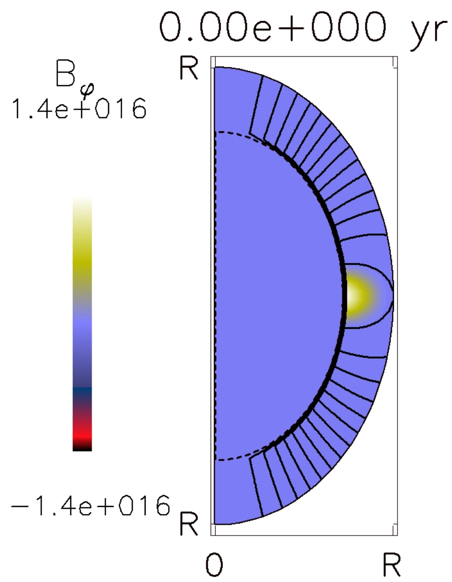

Figure 6: Initial magnetic field structure of a neutron star for the core threaded model.

Both configurations have the same initial symmetric surface temperature distribution in order to enable a simple comparison between the resulting evolutions of the two models. Hot poles are separated by a cold equatorial belt (see figure 5). The initial

maximum and minimum temperatures are $7.7 \cdot 10^6$ K and $4.0 \cdot 10^6$ K respectively.
The magnetic field is visualized in an image showing a cut perpendicular to the equator through the star (see figure 6 as an example). The field lines are shown in black and the B_ϕ component is coloured corresponding to each value.
The B_ϕ component corresponds to the toroidal field component since the poloidal component is independent of ϕ. The evolution of the magnetic field lines is shown for a crust with a thickness of 800 meters. Furthermore the structure of the magnetic field lines is symmetrical around the poles which makes it possible to consider only one half of the intersection.

5.1 Dipolar poloidal and toroidal crustal magnetic field permeating the whole neutron star

In the first, core model the magnetic field is penetrating the whole star. The dipolar poloidal surface field has a strength of $B_p(r = R_{ns}, \theta = 90°, t = 0) = 10^{13}$ G at the poles and the dipolar toroidal field is given with $B_{t,max}(t = 0\ ) = 2 \cdot 10^{16}$ G in the core at the equatorial plain.
At the beginning of the evolution the development of the temperature is similar in both hemispheres with a decreasing overall temperature.
After about 2.000 years the cold equatorial belt shifts from the equator towards the North Pole (see figure 7b). This movement continues for another 200.000 years. After this time a broad cold band is present at angles between 0° and −60° (see figure 7d). This minimum differentiates over the following years to an area of about −10° to −60°. After the simulated approximately $1 \cdot 10^7$ years a maximum with a width of 20° formed around the North Pole while the southern hemisphere stays unaltered in the whole evolution, apart from an overall decrease in the temperature as mentioned before (see figure 7f).
The overall decrease in temperature is shown in figure 8 on page 16. The red coloured line represents the initial temperature distribution from the North to the South Pole (at an angle of −90° and 90° respectively). The blue coloured line shows the final distribution. The maximum temperature at the beginning and at the end of the evolution are $7.7 \cdot 10^6$ K and $1.2 \cdot 10^6$ K respectively. The overall final minimum temperature is $3.6 \cdot 10^5$ K.

Simultaneously to the evolution of the temperature the magnetic field develops as well. The magnetic field structure is symmetric at the beginning. The B_ϕ component has its highest value of $1.4 \cdot 10^{16}$ G at the core-crust boundary at the equator (see figure 7a).

Only a short moment after the start of the calculation the magnetic field lines start to move towards the North Pole (see for example 7b). The magnetic field component B_ϕ varies also to higher values near this point. After about $1.6 \cdot 10^5$ years the development seems to have reached a steady state (see figure 7c). Only very slight transformations are visible considering larger time steps. At an age of $2 \cdot 10^5$ years a huge concentration of field lines is present in the small area around the North Pole of the star which denotes a locally strong magnetic field. At angles of about 0° to −60° closed field lines proceed inside the star parallel to the crust. In the following years the development at the North Pole becomes even more localized (see figure 7e).
During the whole evolution the maximum value of the B_ϕ component decreases by one order of magnitude and the magnetic field does not perform any changes at the area around the South Pole.

Already in the examination of the evolution of the surface temperature distribution and the magnetic field of this model many similarities and consequences of one to the other are visible. The calculations illustrate changes in the overall structure at the same time steps and at the same areas of the star. From these facts one can conclude that the magnetic field has a huge influence on the surface temperature distribution of a neutron star.

Comparing single areas in both distributions one can detect the behaviour explained in section 3 regarding the heat flow parallel to the magnetic field lines. Studying the evolution after $6 \cdot 10^5$ years more closely the dependence can be detected (see figure 7e). In the southern hemisphere of the neutron star the field lines are radial over the whole evolution. This results in a strong heat flow in the area along the magnetic field lines to the surface of the neutron star. Due to the stability of this the temperature in the southern hemisphere has the same distribution over the whole time. The overall decrease in the temperature can be explained by the general cooling of the star.
In the area between the equator and the North Pole the closed magnetic field lines run inside the crust parallel to the surface. The fact that not only one field line but several of them show this behaviour leads to a good isolation and almost no heat reaches the surface. At the same time the high value of the toroidal field component supports the insulating behaviour.
At the point where the magnetic field lines get to the North Pole (at an angle of about −60°) many of these field lines former present in the now isolating area are present due to the shift to the North Pole and proceed radial. The high number of field lines

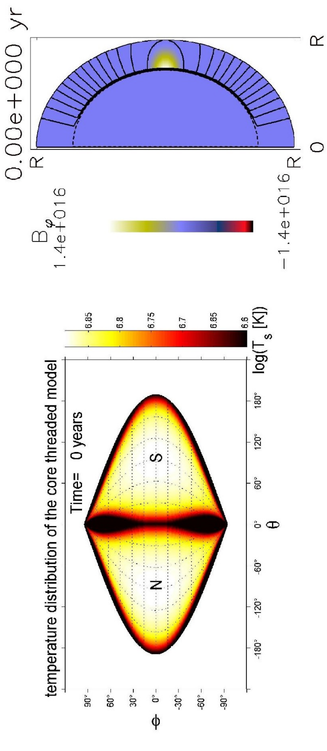

(a) Initial distributions.

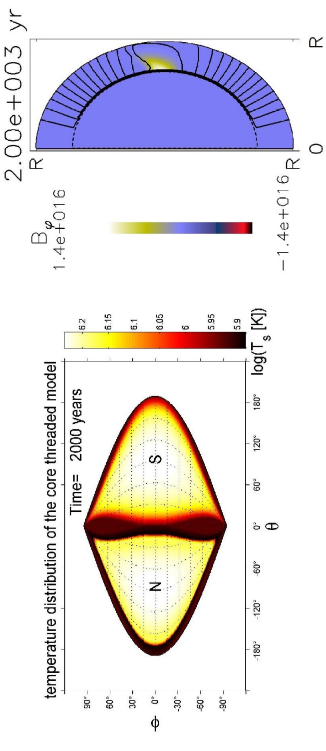

(b) after 2.000 years.

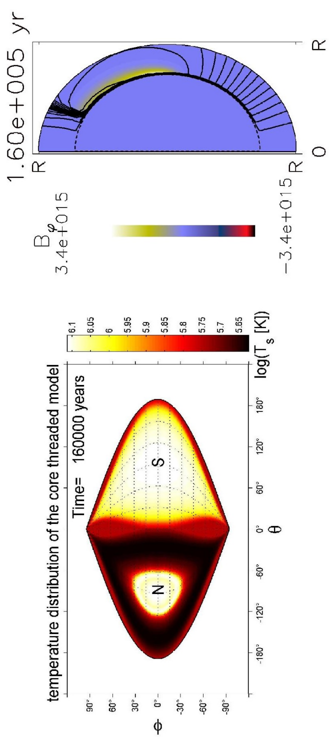

(c) after 160.000 years.

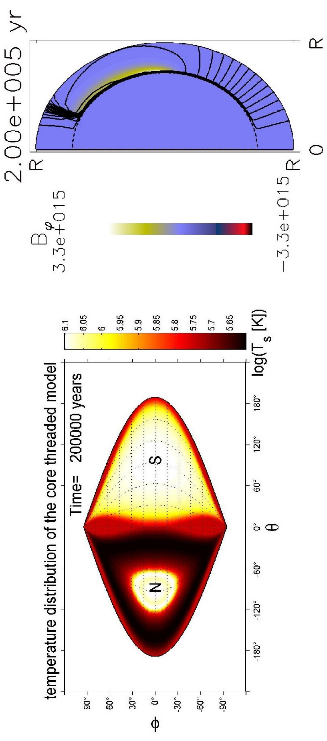

(d) after 200.000 years.

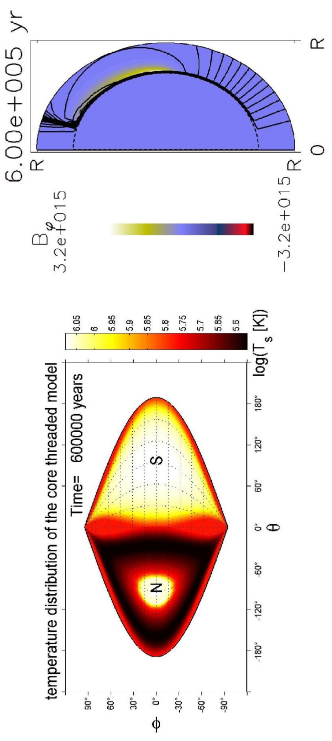

(e) after $6 \cdot 10^5$ years.

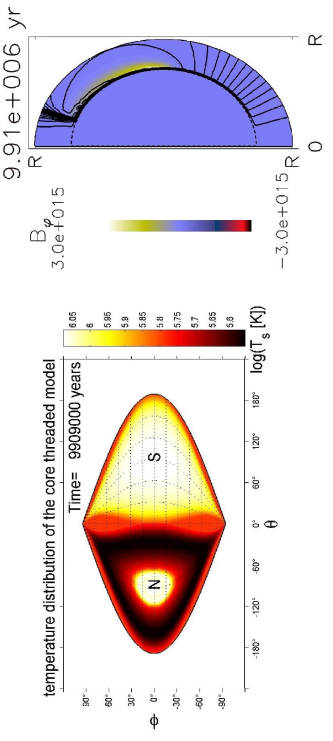

(f) after $9.91 \cdot 10^6$ years.

Figure 7: Temporal evolution of the surface temperature distribution and the magnetic field of a neutron star in case of the core threaded model.

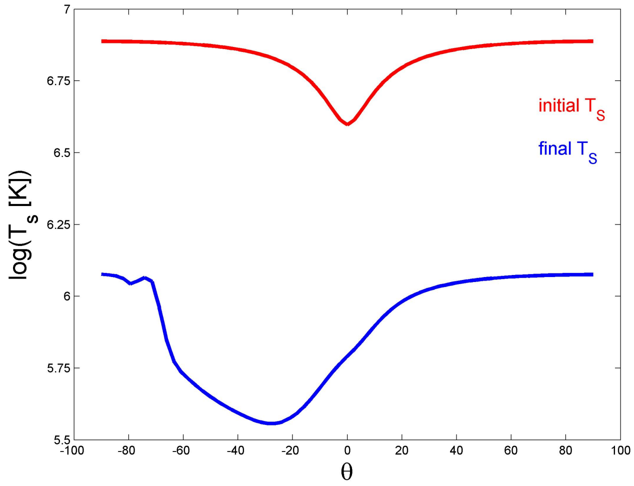

Figure 8: Initial and final temperature distribution of the neutron star in case of the core field.

amplifies the heat flux outwards which leads to the high maximum temperature. This development is further encouraged by the low value of the B_ϕ component.
Considering the minimum in the northern hemisphere (at angles of $-10°$ to $-60°$) it can be detected that a high B_ϕ component suppresses the heat flow. In this area the B_ϕ component has the highest value of about $3 \cdot 10^{15}$ G, whereas the temperature distribution has its lowest values.

5.2 Dipolar poloidal and toroidal crustal magnetic field

The second model considered in this work is a crustal field. The dipolar poloidal and dipolar toroidal components are limited to the crust and reach about 0.8 km far into the neutron star. Moreover the poloidal component proceeds meridional. The initial magnetic field components are given with $B_p(r = R_{ns}, \theta = 90°, t = 0) = 10^{13}$ G and $B_{t,max}(t = 0) = 1.5 \cdot 10^{15}$ G for the poloidal and toroidal component, respectively, which cause many changes in the surface temperature distribution.
The temperature cools down in the first 400 years to a maximal value of $2.0 \cdot 10^6$ K from an initial temperature of $7.7 \cdot 10^6$ K. In this evolutionary state the poles stay warmer than the rest of the neutron star. In the following years the cold belt around the equator moves towards the North Pole until it creates a cold minimum around the pole at an angle of about $-70°$ at an age of 40.000 years. This development can already be seen after 22.000 years (see figure 9b).
Besides that the overall temperature continues to decrease. The minimum in the north-

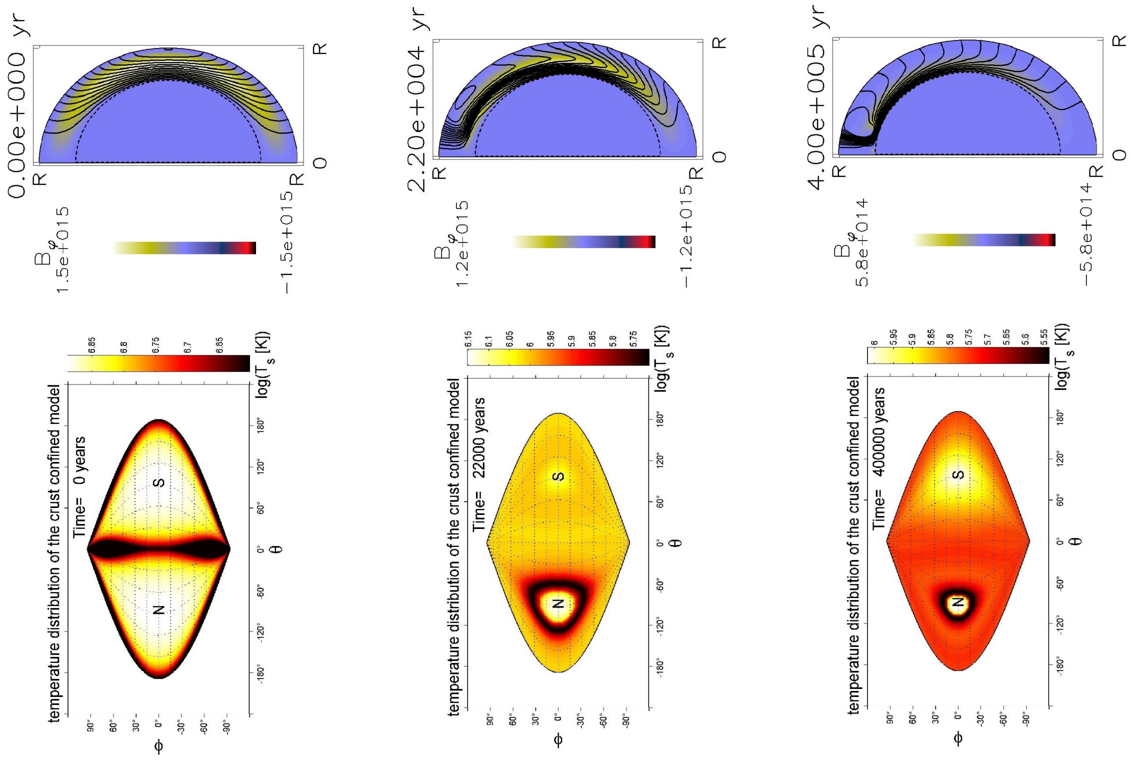

(a) Initial distributions. (b) after 22.000 years. (c) after $4 \cdot 10^5$ years.

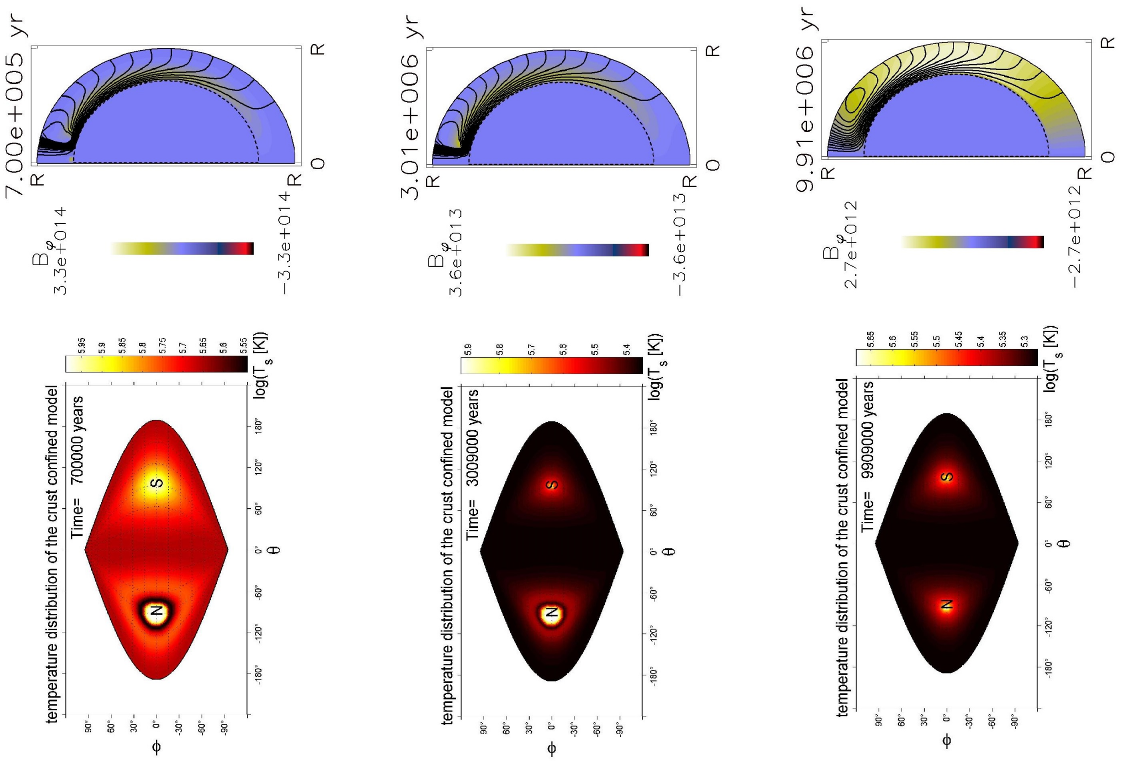

(d) after $7 \cdot 10^5$ years. (e) after $3.01 \cdot 10^6$ years. (f) after $9.91 \cdot 10^6$ years.

Figure 9: Temporal evolution of the surface temperature distribution and the magnetic field of a neutron star in case of the crust confined model.

ern hemisphere becomes more localized and moves to an angle of about $-80°$ with a width of about $10°$ (see figure 9c). A small maximum begins to form at an angle of $-50°$ after 400.000 years. It slightly grows over the years (see figure 9d). At the same time the maximum at the South Pole increases in temperature and becomes more localized (compare figures 9c and 9d). At an age of about 700.000 years a cold equatorial belt starts to form again (see figure 9d). This belt has a width of $60°$ after only 200.000 years of formation.
The cold area spreads to both hemispheres and swallows the first smaller maximum in the northern half of the neutron star. This development starts at an age of $2 \cdot 10^6$ years and continues until only a small maximum at the South Pole and a global maximum at the North Pole dominate the surface temperature distribution after $9.91 \cdot 10^6$ years (see figure 9f).

Corresponding to this evolution changes in the magnetic field are visible.
The initial structure is dominated by the poloidal progression parallel to the crust. The toroidal magnetic field component is distributed symmetrically around the equator (see figure 9a).
In the first evolutionary years the magnetic field lines are compressed into a progressing smaller volume in the northern hemisphere. This corresponds to the strong increase of the local magnetic flux at the North Pole (see figure 9b). At the same time the distance between the magnetic field lines becomes larger at the South Pole. After $4 \cdot 10^5$ years the radial field lines are closely together at the North Pole (see figure 9c). This structure grows very slowly for another $2.8 \cdot 10^6$ years (see figure 9e). The maximum value of the B_ϕ component is located at the core-crust boundary.
Already at the age of $7 \cdot 10^5$ years closed field lines are present near the North Pole and move slightly to the south. In the middle of these developed structures a part of the field lines runs parallel to the crust.
These magnetic field lines seem to under go a slight re-evolution since the structures at the ages of $2.2 \cdot 10^4$ years and $9.91 \cdot 10^6$ years are similar (compare figures 9b and 9f).
The B_ϕ component decreases over the whole temporal evolution but starts to spread onto the whole crust after $5 \cdot 10^6$ years (see figure 9f). At the end of the evolution this component has a maximum value of $2.7 \cdot 10^{12}$ G at the equator.

Comparing these developments, it is detectable that the B_ϕ component leads to the strong cooling of the surface temperature distribution at the end of the evolution. The toroidal magnetic field component has only a comparably low value at the poles which

makes the generation of the high temperature maxima possible due to its geometrical structure.
At the North Pole the magnetic field is not heat-insulating which leads to a hot pole. The maximum is strengthened by the fact that the field lines are perpendicular to the surface in a condensed form. The poloidal component of the field proceeds parallel to the core surface in a compressed form at angles of about $-50°$ to $-80°$ after $2.2 \cdot 10^4$ years (see figure 9b). In addition to the B_ϕ component this also leads to an isolation in the area between $-40°$ to $-80°$ which means that no heat flow from the core to the outside of the star is possible. Further away from the North Pole (at angles of about $-30°$) the isolation weakens as field lines former parallel to the crust change into field lines perpendicular to the surface. The heat is transported parallel to the magnetic field lines as explained in section 3.
As mentioned before, a slightly warmer area begins to form at angles of about $-50°$ at an age of $4 \cdot 10^5$ years (see figure 9c). This is caused by the structure of the magnetic field lines. Next to a small area, where they proceed parallel to the core-crust boundary at $-80°$, some magnetic field lines run perpendicular to the surface at the warmer region. At this point the magnetic field component B_ϕ does not have a significant higher value and thereby does not have a strong isolating feature.

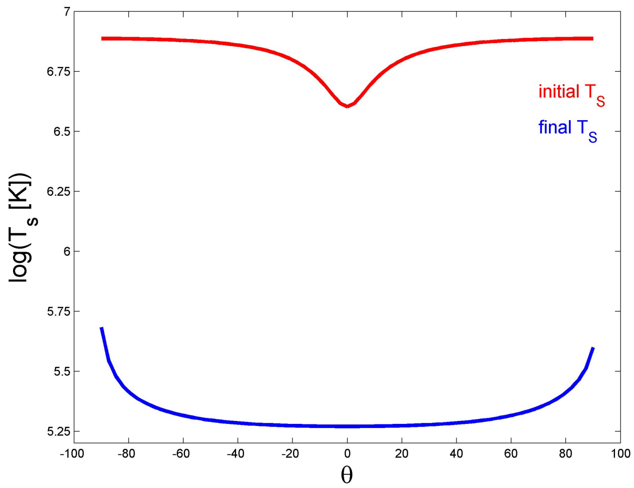

Figure 10: Initial and final temperature distribution of the neutron star in case of the crustal field.

When comparing the surface temperature distribution and the magnetic field structure at the age of $7 \cdot 10^5$ years an abnormality is detectable at the equator. Although a small number of field lines proceed perpendicular to the surface a cold equatorial belt begins to form and grows in intensity over the following years until a stationary state

is reached. These evolutions can be explained by the examination of the B_ϕ field component. This B_ϕ component increases in value at the area around the equator. The structure and concentration of that component leads to the strong outward isolation of the heat flux.
The overall temperature decreases by a factor of about 16 from $7.7 \cdot 10^6$ K to $4.8 \cdot 10^5$ K. Figure 10 shows the initial (red) and final (blue) surface temperature from the North to the South Pole. This development is a characteristic for the model considered in this subsection.

6 Discussion

The previous analysis is based on the requirement that the magnetic field evolves under the influence of Ohmic diffusion and Hall drift. Consequently the magnetic field causes the temporal evolution of the surface temperature distribution.
It becomes obvious in the analysis that different magnetic field structures induce different surface temperature distributions. The resulting final distributions of both models diverge significantly.

The core threaded and the crust confined model both consist of a dipolar poloidal and toroidal component. Already the comparison of the maximum temperatures of the neutron star after $9.91 \cdot 10^6$ years shows a difference. In case of the core threaded model the final maximum temperature is at $1.2 \cdot 10^6$ K, whereas the temperature of the crust confined model is at $4.8 \cdot 10^5$ K. The difference confirms the statement of Geppert et al. (2004) that a crustal magnetic field impedes the heat transfer to the outside, whereas a core magnetic field supports this transfer (see section 3) [6]. In the evolution of the models considered in this work high values in the B_ϕ component and as such in the toroidal component of the magnetic field prevent an outward heat flux. This is seen for example in figure 9e on page 17. Furthermore it is detectable that the radial structure of the magnetic field lines strengthen the heat transfer in the evolution of the core threaded model (southern hemisphere in figure 7f on page 15). The good heat transfer causes the final maximum temperature to be smaller than the initial maximum temperature by only a factor of about 6.5 . This decrease is determined by the overall cooling of the neutron star.
In the model assuming a crustal magnetic field the magnetic field lines are mainly meridional. Magnetic field lines proceed radial only close to the North and South Pole. It is visible that the meridional structure prevents the heat transfer because the overall final surface temperature is significantly lower than in case of the core field.

The toroidal and meridional structures compensate the effect of the heat-transfer-supporting radial structures in the crustal model.

Apart from the different final surface temperatures the surface temperature distributions are diverse as well.
As mentioned in section 4 Geppert (2013) stated that the changes in the magnetic field are caused by the changes in the crustal field since it has a smaller decay time than a core field [11].Comparing the crustal and core model in this work the statement is confirmed. The development of the surface temperature is significantly stronger in case of the crustal magnetic field. Changes in the surface temperature distribution and in the magnetic field structure are visible in both hemispheres, whereas the core field only leads to changes in the northern hemisphere.
Including that the core field consists of a toroidal and a poloidal component in the consideration of the core model, it is surprising that the toroidal component results in only slight changes in the surface temperature distribution. The evolution is possibly determined by the changes in the core threaded poloidal magnetic field component although the toroidal component has similar weaker changes corresponding to it. It is assumed that these weaker changes can be neglected in comparison to the changes in the dipolar poloidal component.

The temporal stability of the magnetic fields and the corresponding surface temperature distributions are different for the core and crustal model. On the one hand the magnetic field lines of the crustal model already formed their final structure after only $1 \cdot 10^5$ years. Subsequently only slight changes occur. On the other hand the toroidal field component is stable for at least $4 \cdot 10^6$ years and high values in this component arise in other areas in the crust at this age or a higher. The core model has the greatest evolutionary steps in the years up to the age of $2 \cdot 10^5$ years. The magnetic field is stable over the remaining calculated time period, apart from negligible progresses.

The final surface temperature distributions of the core and crustal magnetic field differ not only in the different areas in which changes in the temperature profile are visible, but also in the form of the maxima they exhibit. The core model has a maximum in the northern hemisphere, which has a width of about 20°, and a maximum in the southern hemisphere, which encloses almost the whole southern hemisphere of the neutron star. But then the crustal model exhibits only two small maxima, one at the North and one at the South Pole. They are spatial confined and have a width of only a few degrees. The maxima have values of about $4.8 \cdot 10^5$ K which is higher than the surrounding area by a factor of 2.6. The meridional and toroidal field components and field lines lead to a heat flux to the poles and at the same time cause an extended cold equatorial belt. This belt dominates the surface temperature in the remaining areas of the star.

Geppert et al. (2004) further stated that the different surface temperature structures and magnetic fields arouse different X-ray pulse profiles of the pulsating, isolated and strongly magnetized neutron stars [6]. They have an influence on the shape and amplitude of the signal according to their declaration. When one postulates this assumption, a conclusion can be made from the observed neutron star pulses on the thermal and magnetic structure of the star. The calculated and analysed models in this thesis and previous work by others will be the foundation of the future analyses.

7 Conclusion

This work focuses on isolated neutron stars. According to previous work by others the magnetic field of these stars has an influence on the surface temperature distribution. Two models are considered in this work: a core and a crustal field. The difference in these examples is to be found in the area the individual magnetic fields penetrate. These two diverse models cause very different surface temperature distributions when one considers the Hall effect in the calculations. This so-called Hall drift, which originates from the interactions between the magnetic field and the electric currents in the neutron star, has an influence on the evolution of the magnetic field structure which can be seen in the Hall induction equation (see equation 9).

The two surface temperature distributions differ significantly. In case of the core field changes are only visible in the northern hemisphere. The southern hemisphere is dominated by a maximum which includes nearly the whole southern hemisphere. On the contrary the northern hemisphere exhibits a confined maximum at the pole. In case of the crustal field the surface temperature distribution has only two very confined maxima, one at the North and one at the South Pole. These maxima have temperature values much higher than the rest of the neutron star.
The difference results from the structures of the magnetic field in the considered models. The toroidal and meridional magnetic field components tend to hinder the outward heat flux in the crust confined model. They channel the heat to the poles and thereby cause the maxima. However the radial components of the magnetic field encourage the heat flux. This can be clearly seen in the evolution of the southern hemisphere of the core field model.

At the same time these field structures cause different maximum surface temperatures. Just because of the above-mentioned reason not enough heat can flow to the surface of the neutron star in case of the crustal model and heat it up. A discrepancy of about one order of magnitude in the final maximum temperature between the models arises.

Furthermore, the temporal stability of the two magnetic fields varies. A stability after already $2 \cdot 10^5$ years is in contrast to a slight continuous change.

Since the X-ray pulse profile might be affected by the magnetic field and the surface temperature distribution future work may focus on the determination of this relationship [6]. Based on that, the magnetic field structure of observed neutron stars can be detected. Out of the comparison of the observed X-ray pulses or surface temperature profiles and the calculated simulations a consequence can be drawn.
The two models examined in this work are a part of these calculated simulations. A comparison of these with observational data forms the basis for a future analysis.

8 References

[1] Demtröder, W. (2014): Experimentalphysik 4: Kern-, Teilchen- und Astrophysik. - Springer: Berlin, Heidelberg, 4th edition, 339-379.

[2] Kaspi, V. M. et al. (2006): Isolated neutron stars. - In: Compact Stellar X-ray Sources / ed. by Walter Lewin & Michiel van der Klis. – Cambridge astrophysics series 39, Cambridge University Press: Cambridge, 279-340.

[3] Scharringhausen, M. (2014): Abriss der Astrophysik. - Lecture at the University of Bremen. - Summer term 2014. - unpublished.

[4] Baade, W. and Zwicky, F. (1934): Cosmic rays from Super-Novae. - Proceedings of the National Academy of Sciences 20 (5), 259–263. - http://dx.doi.org/10.1073/pnas.20.5.259.

[5] Sathyaprakash, B. S. and Schutz, B. F. (2009): Physics, astrophysics and cosmology with gravitational waves. - Living Review in Relativity 12 (2), 96-99. - http://dx.doi.org/10.12942/lrr-2009-2.

[6] Geppert, U. R. M. E. et al. (2004): Temperature distribution in magnetized neutron star crusts. - Astronomy and Astrophysics 426 (1), 267-277. - http://dx.doi.org/10.1051/0004-6361:20040455.

[7] Shapiro, S. L. and Teukolsky, S. A. (2004): Black Holes, White Dwarfs and Neutron Stars: The physics of compact objects. - Wiley-VCH: Weinheim, 645 pages.

[8] Yakovlev, D. G. and Kaminker, A. D. (1994): Neutron Star crusts with magnetic fields. - In: The Equation of State in Astrophysics / ed. by G. Chabrier & E. Schatzmann. - IAU (International Astronomical Union) Colloquium 147, Cambridge University Press: Cambridge, 214-238.

[9] Kippenhahn, R. et al. (2012): Stellar structure and evolution. - Springer: Berlin, Heidelberg, 2nd edition, 604 pages.

[10] Geppert, U. R. M. E. et al. (2006): Temperature distribution in magnetized neutron star crusts, II. The effect of a strong toroidal component. - Astronomy and Astrophysics 457 (3), 937-947. - http://dx.doi.org/10.1051/0004-6361:20054696.

[11] Geppert, U. R. M. E. (2013): Radio pulsar activity and crustal Hall drift. - Talk at the Center of Applied Space Technology and Microgravity ZARM, University of Bremen. - 16.10.2013. - unpublished.

[12] Viganò, D. et al. (2012): A new code for the Hall-driven magnetic evolution of neutron stars. - Computer Physics Communications, 183 (10), 2042-2053. - http://dx.doi.org/10.1016/j.cpc.2012.04.029.

[13] Geppert, U. R. M. E. et al. (2013): Radio pulsar activity and the crustal Hall drift. - Monthly Notices of the Royal Astronomical Society 435 (4), 3262-3271. - http://dx.doi.org/10.1093/mnras/stt1527.

[14] Yasutake, N. et al. (2014): An investigation into surface temperature distributions of High-B Pulsars. - Publications of the Astronomical Society of Japan 66 (2), 1-22. - http://dx.doi.org/10.1093/pasj/psu009.

[15] Pérez-Azorín, J. F. et al. (2006): Anisotropic thermal emission from magnetized neutron stars. - Astronomy and Astrophysics 451 (3), 1009-1024. - http://dx.doi.org/10.1051/0004-6361:20054403.

[16] Pons, J. A. and Geppert, U. R. M. E. (2010): Confirmation of the occurrence of the Hall instability in the non-linear regime. - Astronomy and Astrophysics 513 (L12), 1-5. - http://dx.doi.org/10.1051/0004-6361/201014197.

[17] Rheinhardt, M. and Geppert, U. R. M. E. (2002): Hall-Drift induced magnetic field instability in Neutron Stars. - Physical review letters 88 (10), 101103, 1-4. - http://dx.doi.org/10.1103/PhysRevLett.88.101103.

A Numerical Codes

A.1 Graphical visualization

```
clear all
close all
clc        % clear comand window

%--------------
n= 69;                          % number of rows in each table
A= load('Ts_core_neu.txt');     % loading of the temperature values
zeilen= size(A,1);              % number of rows in A
ts= zeilen/n;                   % number of time steps

% transformation: every time step is listed in another table, additional
% dimension
B= reshape(A, n, ts, 2);        % new matrix

%--------------
% loading of the data in order to show the corresponding age of the
% star for each time step
dat = fopen('Ts_core_Zeit.txt');  % opening of the file
%---------------

for ii=1:1297                   % end at 1297 (for both models)

% left half/ northern hemisphere -----------------------------
M=zeros(137,137);               % empty matrix for the individual
                          % theta/phi combinations

v=zeros(35,1);                  % vector with the temperature values for
                          % each time step ii
v(1:35,1)= B(1:35,ii,2);

%--------
% linear interpolation between each time step
a=zeros(69,1);                  % expansion vector for v
a(69,1)=v(35,1);
i=1;
j=1;
while i<69 && j<35
    a(i,1)= v(j,1);
    a(i+1,1)= (v(j,1)+v(j+1,1))/2; % linear interpolation
    i=i+2;
```

```
    j=j+1;
end

% ------ central position of the matrix M at:
x= 69;
y= 69;

M(x,y)=a(1,1);

% each combination of k and j with a value higher than
% sqrt(((x-k)^2+(y-j)^2)) becomes the value a(r,1) of the extrapolated
% vector assigned:
for r=1:69
    for k=1:137
        for j=1:137
            if sqrt(((x-k)^2+(y-j)^2))>=r
            M(k,j)= a(r,1);
            end
        end
    end
end

% -----------------------------------------
% right half/ southern hemisphere -----------------
% (corresponding to the northern hemisphere)

w=zeros(35,1);
w(1:35,1)= flipud(B(35:69,ii,2)); % due to the symmetry the values in the
% original matrix have to be switched for the correct visualization

% linear interpolation (see above for details)
b=zeros(69,1);
b(69,1)=w(35,1);
i=1;
j=1;
while i<69 && j<35
    b(i,1)= w(j,1);
    b(i+1,1)= (w(j,1)+w(j+1,1))/2; % linear interpolation

    i=i+2;
    j=j+1;
end

% matrix of the southern hemisphere, corresponding to M
```

```
N=zeros(137,137);

% ---- see above for the documentation
x= 69;
y= 69;

N(x,y)=b(1,1);

for r=1:69
    for k=1:137
        for j=1:137
            if sqrt(((x-k)^2+(y-j)^2))>=r
            N(k,j)= b(r,1);
            end
        end
    end
end

% ------------------------------
% matrices M,N added together
% due to a douple calculation: reduction of matrix N by one column
% new matrix: O= zeros(137,136);
O= N(:,2:137);

% -> matrices M and O added together to form matrix P
P= [M,O];

%------------------------------------------------------------------------
% display of the corresponding time

ende= 1279; % number of rows in dat file with a time value: 1279
D=cell(1279,1);

    C=fgetl(dat);               % reads in the row and
    D(ii,1)=C;                  % saves the content in D(ii,1)
    if ii>=ende                 % end of file dat reached
        break
    end
    for j=1:71                  % skips rows in file dat in which no time
                                        % values are listed
        E=fgetl(dat);
    end

%-----
```

```
% all entries in D up to k are set to be empty
% -> no overlap of the different included texts
k= ii -1;
for j=1:k
    D(j,1)='';
end

% adding of the corresponding time value to the image
h1=text(0.15, 1.75, D(ii,1), 'Color', 'k', 'Fontsize',18);

% ------------------------------------------------------------------------
% overall theta and phi axes, x and y axes respectively
theta= linspace(-180, 180, 273);    % divided in 273 steps
phi= linspace(-90, 90, 137);        % divided in 137 steps


% ------------------------------------------------------------------------
% Sinusoidal Projektion

% system of coordinates
axesm ('sinusoid', 'Frame', 'on', 'Grid', 'on');

% ticks on axes
set(gca,'XTick',-4:1:4, 'YTick', -2:0.5:2, 'TickDir', 'out');
set(gca,'XTickLabel','','-180°','-120°','-60°','0°','60°','120°','180°','', 'YTickLabel',
'','-90°','-60°','-30°','0°','30°','60°','90°','');
% labeling of the poles
text(-1.6, 0, 'N', 'Color', 'k', 'Fontsize',17); % North Pole
text(1.5, 0, 'S', 'Color', 'k', 'Fontsize',17); % South Pole

% colormap adapts the values/ colours at every time step
Cmax= max(P(:));
Cmin= min(P(:));
set(gca, 'CLim', [Cmin, Cmax]);
colormap(hot);

% plot
Z= pcolorm(phi, theta, P);

cb= colorbar('vert'); % orientation of the colorbar (or hori)
zlab = get(cb,'xlabel'); % orientation of the colorbar label (or ylabel)
set(zlab,'String','log(T_s [K])', 'Fontsize',18);

% image labels
```

```
title('temperature distribution of the core threaded model',
'Fontsize',18);
xlabel('\theta', 'Fontsize',20)
ylabel('\phi', 'Fontsize',20)

% -------------------------------------------
% saving the image
writeprefix = '\Users\Sabrina\sonstiges\Documents\Uni\Bachelorarbeit
\Temperaturverteilung_core\Temp_';
    numread1='0000';
    numread1(end-numel(num2str(ii))+1:end) = num2str(ii);
print( '-djpeg', '-r300', [writeprefix numread1])
delete(h1); % deletes text h1 from the image

end
fclose(dat);              % closing of file dat
```

A.2 Synchronization of the surface temperature distribution and the magnetic field

```matlab
clear all
close all
clc                                      % clear comand window
%---------------------------------------------------------------
for ii=1:1279
    kk=ii-1

    % loading of the temperature and the magnetic field images
 numread1='0000';
  numread1(end-numel(num2str(kk))+1:end) = num2str(kk);
  name1= strcat('\Users\Sabrina\sonstiges\Documents\Uni\Bachelorarbeit
  \Magnetfeld_Darstellung\IMAGES_crust_richtig\bcrust', numread1);
  name2= strcat('\Users\Sabrina\sonstiges\Documents\Uni\Bachelorarbeit
  \Temperaturverteilung_crust_richtig\Temp_', numread1);
    Y= imread(name1,'jpg');              % image of the magnetic field
    X= imread(name2, 'jpg');             % image of the temperature
    %-----------------------------------

    % assembly of both images
    figure
     subplot(1,2,1);
     plot1= image(X);
     set(gca, 'Visible', 'off');                    % fading out of the axes
     set(gca, 'Position', [0 0.2 0.5 0.55]);        % amplification of the axes
     set(gcf, 'PaperPositionMode', 'manual');       % definition of output size

     % display of the image, 1:1
     set(gcf, 'Position', [25 25 size(X, 2) size(X, 1)]);

     subplot(1,2,2);
     plot2= image(Y);

    %-----------------------------------
    %-- editing of the axes
    set(gca, 'Visible', 'off');                     % fading out of the axes
    set(gca, 'Position', [0.5 0.2 0.3 0.5]);        % amplification of the axes
    set(gcf, 'PaperPositionMode', 'manual');        % definition of output size
    % Bild 1:1 darstellen
    set(gcf, 'Position', [5 5 size(Y, 2) size(Y, 1)]);

    % storage of the new image (with new name)
```

```
    kk=ii -1;
    writeprefix = '\Users\Sabrina\sonstiges\Documents\Uni\Bachelorarbeit\
    Temp_B-Feld_synchr\synchr';
    numread1='0000';
    numread1(end-numel(num2str(kk))+1:end) = num2str(kk);
    print( '-djpeg', '-r300', [writeprefix numread1])
end
```

A.3 Initial and final surface temperature distribution

```
clear all
close all
clc

n= 69;                          % number of rows in each table
A= load('Ts_core_neu.txt');     % loading of the temperature values
zeilen= size(A,1);              % number of rows in A
ts= zeilen/n;                   % number of time steps

% transformation: every time step is listed in another table,
% additional dimension
B= reshape(A, n, ts, 2);        % new matrix

ii=1;
    v=zeros(69,1);              % vector with the temperature values for
    % each time step ii
    v(1:69,1)= B(1:69,ii,2);     w(1:69,1)= B(1:69,1297,2);
%----------
% linear interpolation between each time step
a=zeros(137,1);             b=zeros(137,1);      % expansion vector for v/w
a(137,1)=v(69,1);           b(137,1)=w(69,1);

i=1;
j=1;
while i<137 && j<69
    a(i,1)= v(j,1);    b(i,1)= w(j,1);
    a(i+1,1)= (v(j,1)+v(j+1,1))/2; % linear interpolation
    b(i+1,1)= (w(j,1)+w(j+1,1))/2;
    i=i+2;
    j=j+1;
end


theta= linspace(90, -90, 137);

plot(theta, a, 'r')
hold on
plot(theta, b, 'b')

% image labels
% title('Initial and final temperature distribution of the core
% threaded model', 'Fontsize',20);
xlabel('\theta', 'Fontsize',20)
```

```
ylabel('log(T_s [K])', 'Fontsize',20)

set(gca,'xtick',-100:20:100,'ytick',-5.5:0.25:7);
% ------------------------------
% saving the image
writeprefix = '\Users\Sabrina\sonstiges\Documents\Uni\Bachelorarbeit\
Temperature_initial_final_';
    numread1='0000';
    numread1(end-numel(num2str(ii))+1:end) = num2str(ii);
print( '-djpeg', '-r300', [writeprefix numread1])
```

Diese Erklärungen sind in jedes Exemplar der Abschlussarbeit mit einzubinden.

Eidestattliche Erklärung

Blatt der Universität

Name: Sabrina Gronow Matrikel-Nr.: 2693611

Urheberrechtliche Erklärung

Erklärung gem. § 10 (10) Allgemeiner Teil der BPO vom 27.10.2010

Hiermit versichere ich, dass ich meine Bachelorarbeit ohne fremde Hilfe angefertigt habe, und dass ich keine anderen als die von mir angegebenen Quellen und Hilfsmittel benutzt habe.

Alle Stellen, die wörtlich oder sinngemäß aus Veröffentlichungen entnommen sind, habe ich unter Angabe der Quellen als solche kenntlich gemacht.

Die Bachelorarbeit darf nach Abgabe nicht mehr verändert werden.

Datum: ________________ Unterschrift: ______________________

Erklärung zur Veröffentlichung von Abschlussarbeiten

Bitte auswählen und ankreuzen:

- o Ich bin damit einverstanden, dass meine Abschlussarbeit im Universitätsarchiv für wissenschaftliche Zwecke von Dritten eingesehen werden darf.
- o Ich bin damit einverstanden, dass meine Abschlussarbeit nach 30 Jahren (gem. §7 Abs.2 BremArchivG) im Universitätsarchiv für wissenschaftliche Zwecke von Dritten eingesehen werden darf.
- o Ich bin nicht damit einverstanden, dass meine Abschlussarbeit im Universitätsarchiv für wissenschaftliche Zwecke von Dritten eingesehen werden darf.

Datum: ________________ Unterschrift: ______________________

Attachment: DVD containing the videos and codes